Cell Reports
Physical Science

CellPress
OPEN ACCESS

Article

Structure-property correlation in stabilizing axial magnetic anisotropy in octahedral Co(II) complexes

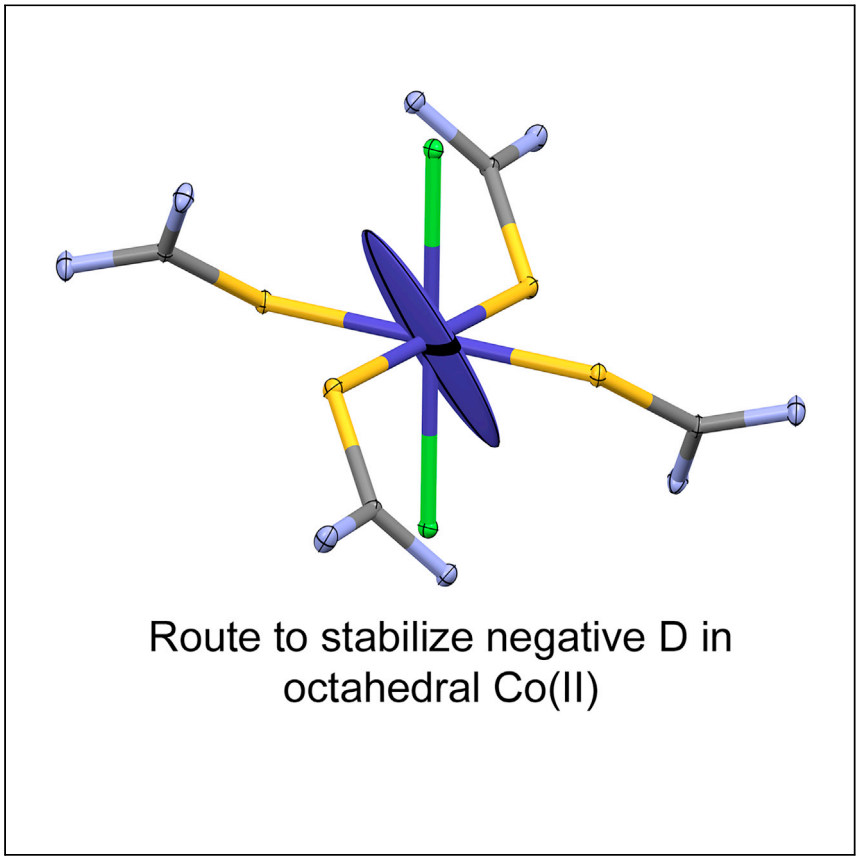

Stabilizing the easy axis of magnetization of octahedral Co(II) complexes that are thermodynamically and air stable is an uphill process. Tripathi et al. report a complex that not only overcomes the impediments in stabilizing negative D but also disclose the parameters that control the sign and magnitude of D.

Shalini Tripathi, Shefali Vaidya, Naushad Ahmed, ..., Gopalan Rajaraman, Jacob Overgaard, Maheswaran Shanmugam

ruediger.klingeler@kip.uni-heidelberg.de (R.K.)
rajaraman@chem.iitb.ac.in (G.R.)
jacobo@chem.au.dk (J.O.)
eswar@chem.iitb.ac.in (M.S.)

Highlights

A synthesized $\{CoS_4Cl_2\}$ complex reveals design principles for stable negative D

The SH parameters were confirmed by high-field pulse magnetization measurements

The sign of D is determined unambiguously by polarized neutron diffraction

Magneto-structural correlations developed by *ab initio* methods unveil the origin of D

Tripathi et al., Cell Reports Physical Science *2*, 100404
April 21, 2021
https://doi.org/10.1016/j.xcrp.2021.100404

Cell Reports
Physical Science

CellPress
OPEN ACCESS

Article

Structure-property correlation in stabilizing axial magnetic anisotropy in octahedral Co(II) complexes

Shalini Tripathi,[1] Shefali Vaidya,[1,6] Naushad Ahmed,[1] Emil Andreasen Klahn,[2] Huibo Cao,[3] Lena Spillecke,[4] Changhyun Koo,[4] Sven Spachmann,[4] Rüdiger Klingeler,[4,5,*] Gopalan Rajaraman,[1,*] Jacob Overgaard,[2,*] and Maheswaran Shanmugam[1,7,*]

SUMMARY

Stabilizing an easy axis of magnetization in an octahedral Co(II) complex is an extremely challenging task, which is evident from reports that more than 90% possess easy-plane anisotropy. Here, we report a six-coordinate complex, $[Co(L_1)_4(Cl)_2]$ (1, L_1 = thiourea [H_2N-CS-NH_2]), that exhibits a D value of $-63(10)$ cm^{-1}. The presence of an easy axis of magnetization associated with 1 is experimentally proven by detailed magnetic studies and polarized neutron diffraction studies, and the experimental observations are well corroborated by theoretical calculations. From the combined experimental and theoretical investigations (on 1 and many model systems), we unveil the parameters that control stabilization of negative D in a thermodynamically favorable and air-stable Co(II) ion in the common distorted octahedral geometry. This study paves the way for overcoming the current impediments to alleviate the easy axis of magnetization using rational ligand choice.

INTRODUCTION

Slow relaxation of magnetization results when the ground state (S) of a metal complex is associated with large easy-axis or Ising-type magnetic anisotropy (D).[1–4] Such complexes show the signature of classic magnet-like behavior (i.e., a hysteresis loop) but, at the same time, exhibit quantum phenomena such as quantum coherence, quantum tunneling of magnetization (QTM), etc.[5–8] Therefore, these complexes can be envisaged for various potential applications, such as high-density information storage, solid-state devices in quantum computing, spin valves, spin filters, etc.[4,9–13] Practical realization of these applications is hampered severely by the low blocking temperature (T_B; the temperature below which slow relaxation of the magnetization phenomenon is observed) exhibited by these complexes.[1,14] Assuming a dominant Orbach relaxation process, T_B is correlated with the barrier height for magnetization reversal $U = |D|S^2$ (for the integer spin state) or $|D|(S^2\text{-}1/4)$ (for the non-integer spin state). Increasing D and S simultaneously is an impossible task.[15–19] For example, the largest Ss, S = 91 and S = 60, known for $Ni_{21}Gd_{20}$ and $Fe_{10}Gd_{10}$, respectively, and other related oligomeric complexes are found to exhibit small Ds.[20–23] This is partly due to the random orientation of the easy magnetic axes of the individual metal ions in the oligomeric complexes. Conversely, some smaller clusters, such as Mn_6, exhibit large D and record-high energy barriers[24]

[1]Department of Chemistry, Indian Institute of Technology (IIT) Bombay, Powai, Mumbai, 400076 Maharashtra, India

[2]Department of Chemistry, Aarhus University, Langelandsgade 140, 8000 Aarhus C, Denmark

[3]Neutron Scattering Division, Oak Ridge National Laboratory, Oak Ridge, TN 37831, USA

[4]Kirchhoff Institute for Physics, Heidelberg University, 69120 Heidelberg, Germany

[5]Centre for Advanced Materials, Heidelberg University, 69120 Heidelberg, Germany

[6]Present address: Université Lyon, Université Claude Bernard Lyon 1, UMR 5256 CNRS, Villeurbanne, France

[7]Lead contact

*Correspondence: ruediger.klingeler@kip.uni-heidelberg.de (R.K.), rajaraman@chem.iitb.ac.in (G.R.), jacobo@chem.au.dk (J.O.), eswar@chem.iitb.ac.in (M.S.)

https://doi.org/10.1016/j.xcrp.2021.100404

In mononuclear systems with more than one unpaired electron, the S of the metal ion often exhibits large single-ion D.[25] As a consequence, slow relaxation of magnetization is observed even for a mononuclear Fe(II) complex, as reported by Harman et al.[25] After this finding, research on mononuclear transition metal systems exploded, particularly to understand the mechanism of magnetization relaxation in larger oligomeric complexes. Another intensive area of research in mononuclear single-molecule magnets (SMMs) based on transition metals is how to control the magnitude of D. For 3d metal ions, this is an extremely challenging task because of quenching of the orbital angular momentum by the ligand field.

A unique strategy to gain orbital angular momentum (to increase the single-ion D) is isolation of coordinatively unsaturated metal complexes. Such an approach has proven fruitful in several two-coordinate Fe(I), Co(II), and Ni(I) complexes, where record anisotropic barrier heights for reversal of magnetization have been reported.[26–30] Although these coordinatively unsaturated metal complexes improve our understanding of the mechanism of slow relaxation of magnetization, their inherent reactive nature and ambient instability makes these complexes unattractive for realization of molecularly based information storage devices. Therefore, an air-stable transition metal SMM with high T_B is in high demand. In general, transition metal complexes with coordination numbers of 4 or more are observed to be air and thermodynamically stable compared with the lower coordination numbers. Furthermore, the literature is dominated by Co(II)-based single-ion magnets (SIMs) compared with other transition metal ions because of its inherent electronic structure; i.e., the Co(II) ion exhibits a non-integer spin system where time reversal of magnetization is not allowed without an applied external perturbation, according to Kramers theorem.[14,31–37]

Among the thermodynamically stable Co(II) complexes, magnetostructural correlations have been developed for the four- and five-coordinate systems to control single-ion anisotropy, whereas similar studies for six-coordinate Co(II) complexes are extremely scarce in the literature, to the best of our knowledge.[34,36–50] Through continuous and systematic studies of a series of tetrahedral Co(II) complexes, it is now well understood that the various factors that may stabilize the largest $M_s = \pm S$ level as a ground Kramers doublet of S = 3/2 system are (1) that the coordination sites of Co(II) are completed by soft donors such as S, P, and As (first coordination sphere);[36,50] (2) peripheral substituents on the ligand (second coordination sphere);[34,35] (3) cation- or anion-induced distortion on Co(II) geometry mediated through supramolecular interactions;[46,51,52] and (4) a ligand that ultimately enforces an ideal D_{2d} symmetry, irrespective of the donor atom types.[34]

Similarly, systematic investigations have foreseen that a ligand that enforces C_3 or C_{3v} symmetry for a five-coordinate Co(II) complex leads to easy-axis D.[41,45,53–56] In addition, it has been proposed to modulate the magnitude of D (in C_3 or D_{3h} symmetry) by maintaining strong σ donors at the axial position and π donors at the equatorial sites.[34,42,44,45] In tetrahedral and trigonal bipyramidal geometry, the ground state electronic configuration does not possess first-order orbital angular momentum, and, therefore, the magnitude of D depends on the extent of mixing of the ground state with the excited states. This is purely governed by the distortion from the ideal geometries and, thus, limits the value of D that could be accomplished.

In contrast to four- and five-coordinate complexes, six-coordinate (octahedral and trigonal prismatic) complexes possess non-zero orbital angular momentum in their ground state electronic configuration; hence, these complexes are expected to

show large D.[31,33,57,58] Among the six-coordinate Co(II) complexes, the trigonal prism geometry is observed to always be stabilized with large negative D, which has been well documented.[52,59–62] However, stabilizing a trigonal prism geometry requires an appropriate ligand design. In this respect, clathrochelate-type ligands are best, but the major problem associated with these ligands is that they often exhibit spin-crossover phenomenon; stabilizing a high spin state in the entire temperature range is a challenging task.[60,63] On the other hand, numerous distorted octahedral Co(II) complexes are reported in the literature,[33,58,64] of which more than 90% are stabilized with easy-plane anisotropy irrespective of any coordinating atoms (Table S1). In this aspect, Deng et al.[65] have shed light on the influence of axial ligand/distortion in modulating single-ion anisotropy of Co(II) six-coordinate complexes.[65]

Nevertheless, there are few studies on stabilizing axial anisotropy in octahedral Co(II) complexes,[64] even though such geometry may lead to first-order orbital angular momentum and, thus, large D. Particularly, there are no investigations to control the sign and magnitude of D of Co(II) six-coordinate complexes using the correct choice of ligand, to the best of our knowledge. A common choice of ligand system consists of hard donor atoms, such as oxygen or nitrogen;[31,66,67] soft donor ligands are rarely used and, when found, not magnetically characterized.[68–71]

Keeping in mind all of these factors, we sought to unveil a synthetic approach to stabilize axial anisotropy in a six-coordinate Co(II) complex. Here we report a mononuclear distorted octahedral complex with the molecular formula $[Co(L_1)_4(Cl)_2]$ (**1**, L_1 = thiourea [H_2N-CS-NH_2]) stabilized with the largest axial D and also disclose a general strategy to stabilize negative D by the correct choice of ligand in a targeted manner. The presence of an easy axis of D in **1** was confirmed by detailed magnetic studies and supported by polarized neutron single-crystal diffraction studies. The detailed electronic structure of **1** and its experimental observations are well corroborated with theoretical calculations (*vide infra*).

RESULTS AND DISCUSSION

Synthesis and characterization of 1

The reaction of cobalt chloride hydrate with L_1 in alcoholic solution led to isolation of blue single crystals (Scheme S1) of the targeted complex upon crystallization from hot ethyl acetate. Single-crystal X-ray diffraction reveals that it is a mononuclear cobalt(II) complex with the molecular formula $[CoCl_2(L_1)_4]$, (**1**; Figure 1). **1** crystallizes in the tetragonal space group $P4_2/n$ (Table 1; Experimental procedures), with the cobalt occupying a special position with site symmetry −1. The asymmetric unit thus consists of half a molecule. The crystal structure of **1** has been reported previously by O'Connor and Amma[72] (Cambridge structural database (CSD) code CTHUCO10), but no other studies have been performed on this molecule. The coordination geometry of Co(II) is a distorted octahedral, with the four equatorial sites occupied by thiourea molecules and the two axial sites occupied by chlorides.

The symmetry enforces the exact linearity of all *trans*-coordinated ligands; i.e., for Cl1-Co1-Cl1#, S1-Co1-S1#, and S2-Co1-S2#, where # indicates the atom related by inversion symmetry. The remaining angles S1-Co1-S2 (87.7°), S1-Co1-Cl1 (92.3°), and S2-Co1-Cl1 (95.5°) deviate slightly from ideal orthogonality.

The weakly distorted octahedral geometry of **1** is quantified by its small continuous shape measurement (CShM) value of 0.21 (Table S2).[73] The CShM value of zero

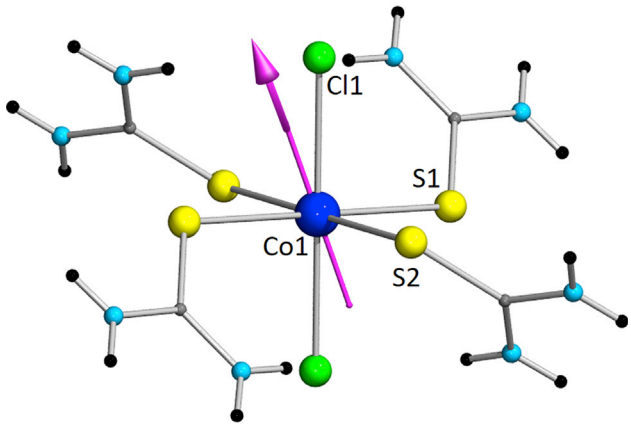

Figure 1. Single-crystal X-ray diffraction structure of 1

The ball and stick diagram shows the crystal structure of 1. Blue, Co; yellow, S; green, Cl; sky blue, N; gray, C; black, H. Selected bond lengths of **1**: Co1-S1, 2.5042(5); Co1-S2, 2.5473(6); Co1-Cl1, 2.4594(2). Bond angles: S1-Co1-Cl1, 92.3(2); S2-Co1-Cl1, 84.5 (2); S1#-Co1-Cl1, 87.7 (2); S2#-Co1-Cl1, 95.5(2). The arrow represents the computed D_{zz} orientation of **1** from *ab initio* calculation.

represents the ideal octahedral geometry, whereas a non-zero CShM value and its magnitude depend on the extent of deviation from ideal octahedral geometry. In **1**, the axial bond distance (Co1-Cl1 = 2.4594(2) Å) is shorter than the equatorial bond distances (Co1-S1 = 2.5042(5) Å and Co1-S2 = 2.5473(6) Å); therefore, **1** is a rare example of a compressed octahedral geometry.[74–76] This unusual geometry observed around the Co(II) ion changes the electronic structure and the related magnetic properties (*vide infra*). Selected bond distances and angles are given in the legend of Figure 1.

All molecules in the crystal lattice orient in the same direction; i.e., the Cl1-Co1-Cl1# axis (which we call the molecular axis; it forms an angle of approximately 85° with the plane spanned by the four equatorial sulfur atoms) of all molecules is oriented roughly along the c axis (Figure 1).

The amide NH_2 groups are efficient hydrogen bond donors, and extensive hydrogen bonding is therefore expected in **1** (Figure 2). Intramolecular hydrogen bonds are found with the axial chlorides ($d_{(N2\cdots Cl1)}$ = 3.2413(1) Å, N2-H2B-Cl1 = 159.2°), whereas several intermolecular hydrogen bonds are mediated via chloride and sulfur with H atoms of L_1. Judging from the N···Cl/S distances, the hydrogen bonding to halide donors is relatively stronger than that to sulfur donors. The shortest intermolecular Co···Co distance observed within the crystal lattice of **1** is 8.081(1) Å. A complete list of hydrogen bonds is given in Table S3, as well as an analysis of the intermolecular interactions.

Direct current magnetization

Variable-temperature direct current (DC) magnetic measurements were performed on polycrystalline-fixed powder sample of **1** in the temperature range of 1.8–300 K in the presence of an external magnetic field of 10 kOe. As shown in Figure 3A, the observed room temperature $\chi_M T$ value for **1** (2.98 cm^3 K mol^{-1}) is significantly larger than the theoretical value for an S = 3/2 case (i.e., 1.875 cm^3 K mol^{-1}; with g = 2), as expected for Co(II) complexes. Furthermore, the observed value is in agreement with other results reported in the literature.[31,77,78] Upon cooling, $\chi_M T$ decreased almost linearly to about 75 K. Below this temperature, $\chi_M T$ decreases

Table 1. Selected crystallographic details for 1 from X-ray diffraction and non-polarized neutron diffraction

	From X-Ray diffraction	From PND
Empirical formula	$CoCl_2(SCN_2H_4)_4$	$CoCl_2(SCN_2H_4)_4$
Formula weight (g mol^{-1})	434.32	434.32
Crystal system, space group	Tetragonal, $P4_2/n$	Tetragonal, $P4_2/n$
Radiation/peak wavelength (Å)	MoK_α/0.71073	neutrons/1.3
a (Å)	13.4516(5)	13.4276(1)
c (Å)	9.0298(5)	8.9885(1)
V ($Å^3$)	1633.90(15)	1620.63(3)
Z	4	4
ρ (g cm^{-3})	1.77	1.78
Completeness (%)	99.6	81
Temperature (K)	100	4
R1 (%)	0.0193	0.0681
wR2 (%)	0.0506	26.4
GoF	1.048	0.773

more rapidly and reaches a low-temperature value of 0.83 cm^3 K mol^{-1} at 1.8 K (Figure 3A).

The magnetic field dependence of the magnetization studied in external static magnetic fields up to 140 kOe at a temperature of T = 2 K (open black circles in Figure 3B) as well as in a pulsed field up to 555 kOe (blue solid line) is presented in the inset in Figure 3A. Additional measurements were performed in magnetic fields up to 70 kOe at several temperatures (Figure S1). Upon application of the external magnetic field, the magnetization rises steeply to B = 50 kOe, followed by a much flatter linear increase without indication of saturation even up to 555 kOe. Furthermore, the maximal measured moment of 3.2 μ_B is significantly lower than the saturation magnetization $M_{sat} = g_{iso}S = 3.66\ \mu_B$, which is expected from g_{iso} obtained from the calculated g tensor below.

The rapid decrease of the $\chi_M T$ value at low temperatures as well as the linear increase of the magnetization with rising magnetic fields without reaching M_{sat} strongly implies the presence of a high axial anisotropy of the crystal field that acts on the Co(II) moments. This is corroborated by the non-superimposable nature of the reduced magnetization data of **1** (Figure S1). To quantify the crystal field parameters, we performed simulations on the field (M(B)) and the temperature dependence ($\chi T(T)$) of the magnetization, considering the following spin Hamiltonian (SH; Equation 1), where g denotes the isotropic g value, μ_B the Bohr magneton, B the external magnetic field, and D and E the axial and transversal anisotropy parameter, respectively.[65,79] The following SH is a good model to simulate the experimental magnetic data because the symmetry around Co(II) is not strictly octahedral in **1**.[22,80–83] For the ideal octahedral (homoleptic ligand) complexes, the spin-orbit coupling is expected to be strong; therefore, L and S formalism should be included when modeling the magnetic data of the complexes.

$$H = g\mu_B \vec{B}\vec{S} + D\left[S_z^2 - \frac{S(S+1)}{3}\right] + E\left(S_x^2 - S_y^2\right) \qquad \text{(Equation 1)}$$

The simulation results are shown as red solid lines in Figure 3. To avoid overparameterization, the |E/D| = 0.22 ratio was fixed to the calculated result, and only D and g were varied. The best simulation parameters are D = −63(10) cm^{-1}, $g_{\chi T}$ = 2.53(5), and g_{MB} = 2.7(1). The different g values obtained for the $\chi_M T(T)$ and M(B) data reflect

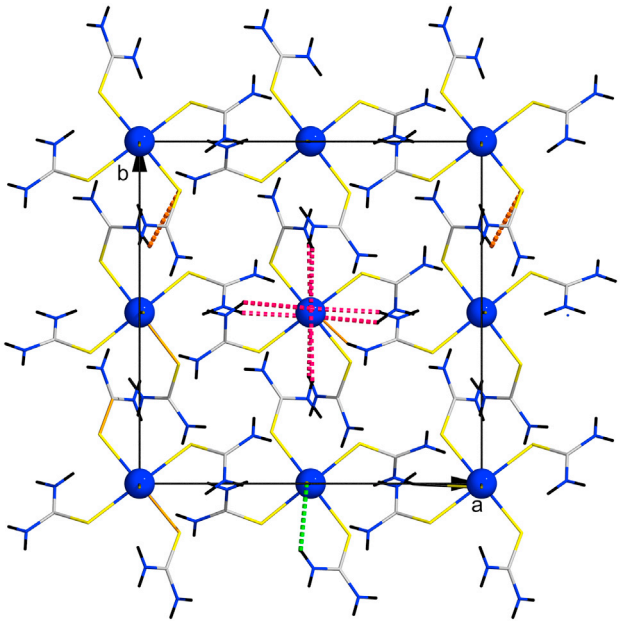

Figure 2. The packing diagram of 1 viewed along the c axis
The inter (dotted pink and orange bonds) and intramolecular (dotted olive green) H-bonding within the crystal lattice of **1**. The same color code for the atoms was used as in Figure 1.

the fact that $g_{\chi T}$ is mainly determined by the room-temperature value of $\chi_M T$ (i.e., it refers to the isotropic g value of the system), whereas g_{MB} is dominated by the component of g, which points along the anisotropy axis of the, in general, anisotropic g tensor and is less dependent on the other components. However, a simulation using an anisotropic g value leads to overparameterization because the M_{sat} has not been reached in the accessible field of 555 kOe.

Although the high temperature and high magnetic field ranges are well described by the respective optimized parameter sets, the data clearly diverge on lower-energy scales. Especially the diminished slope of low-field magnetization (Figure 3B) compared with the simulation implies an influence of antiferromagnetic intermolecular interactions. Closer investigation of the molecular packing scheme shown in Figure 2 as well as Figure S2 supports a scenario of three-dimensional magnetic coupling between the nearest neighboring Co(II) moments mediated via hydrogen bonds. To estimate the strength of the inter-molecular antiferromagnetic interactions, we performed quantum Monte Carlo (QMC) simulations on a cubic lattice with an edge length of L = 10 Å.To reduce the dimensionality of the system, we approximated the localized Co(II) moments as Ising spins of the length $S_z = 3/2$, which is well justified at low magnetic fields and temperatures where only the $m_S = \pm 3/2$ Kramers doublet is populated significantly because of the high zero field splitting induced by axial anisotropy.[84] Thus, the exchange coupling Hamiltonian can be written as[85]

$$H = -J\sum_{\langle i,j\rangle} \overrightarrow{S}_i^z \overrightarrow{S}_j^z \qquad \text{(Equation 2)}$$

The simulation results are shown as blue filled squares in Figure 3B. The experimental data (open black circles in Figure 3B) are well described by the simulation, with a coupling constant J = −0.45(5) K in the magnetic field range below 50 kOe. The effective g value is fixed to $g_z = 3.06$, which is the maximum component of the calculated g tensor described below. As expected, because of the

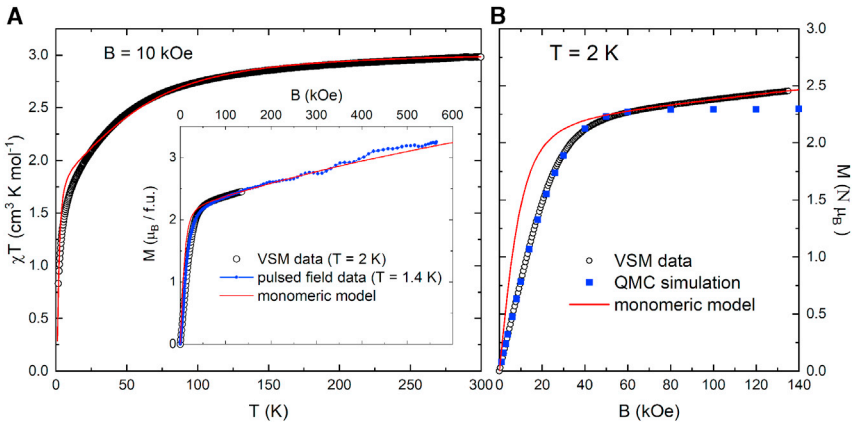

Figure 3. Magnetic characterization of complex 1

(A) Temperature dependence of the DC magnetic susceptibility measured on a polycrystalline sample of **1** in an external magnetic field of 10 kOe (open black symbols). Inset: pulsed-field magnetization on **1** at T = 1.4 K. The pulsed-field data are scaled to static-field data obtained at T = 2 K (open black symbols).

(B) Magnetic field dependence of DC magnetization at T = 2 K (open black symbols). Filled blue squares show QMC simulation results as described in the text. Solid red lines in all plots represent simulations using a monomeric model for $\chi_M T(T)$ and M(*B*), respectively, with the parameters described in the main text.

Ising spin approximation used, the QMC simulation result diverges from the experimental data with increasing fields, where the influence of finite anisotropy becomes non-negligible.

Single-crystal polarized neutron diffraction (PND)

Because there is only one Co atom in the asymmetric unit of **1**, the model with which to refine the PND data only incorporates one magnetic susceptibility tensor. With the intrinsic inversion symmetry of the magnetic susceptibility tensor, this means that a total of 6 parameters are refined from the PND data. Initial refinements, however, showed large correlations between the χ_{11} and χ_{22}-elements, so a constraint was introduced to keep them identical so that the refined magnetic susceptibility tensor for the Co site (given in an orthonormal reference frame coinciding with the crystallographic axes[86]) reduces to

$$\boldsymbol{\chi}_{Co} = \begin{bmatrix} 0.31(2) & 0.09(23) & -0.03(22) \\ 0.09(23) & 0.31(2) & 0.29(17) \\ -0.03(22) & 0.29(17) & 0.55(9) \end{bmatrix} \left[\mu_B\, T^{-1}\right]$$

Diagonalization of this tensor yields the eigenvalues 0.748 $\mu_B\, T^{-1}$, 0.346 $\mu_B\, T^{-1}$, and 0.083 $\mu_B\, T^{-1}$. The $\boldsymbol{\chi}^2$-values for the refinement are 1.94, 1.93, 15.0, 26.4, and 6.5 for orientations 1, 2, 3, 4, and combined (Table S4), respectively. The magnetic susceptibility tensor clearly shows the axial D of **1**; the magnetic susceptibility along the easy axis is roughly a factor of two larger than the second-largest element and a factor of 9 larger than the smallest eigenvalue of the tensor. Indeed, it recovers the strong rhombic term, as also found from DC magnetic susceptibility measurements.

Visualization of the $\boldsymbol{\chi}_{Co}$ tensor on top of the molecular structure is given in Figure 4, showing the pronounced prolate character we identify with easy-axis D and a negative zero-field splitting parameter, in agreement with the magnetic data analysis. Surprisingly, the magnetic easy axis is tilted with respect to the symmetry axis of

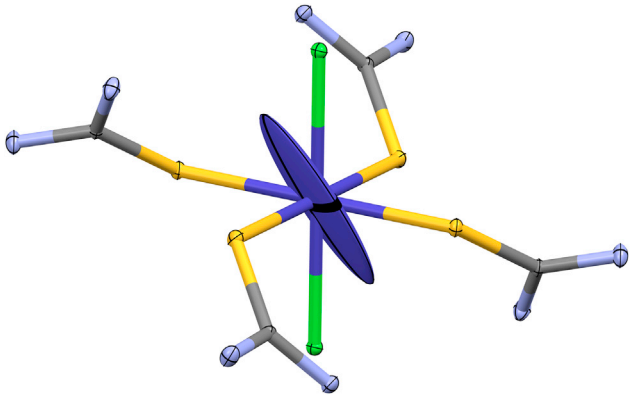

Figure 4. Polarized neutron diffraction measurement performed on a single crystal of 1
Shown is the magnetic susceptibility tensor, visualized as an ellipsoid, overlaid on the molecular structure of **1**. The ellipsoid was scaled arbitrarily to fit onto the molecular structure. The relative magnitudes of the primary axes of the ellipsoid reflect the relative eigenvalues of the corresponding eigenvectors. Co, royal blue; S, yellow; N, blue; C, dark gray.

the ideal octahedral coordination. The angle between the Co-Cl^{-} bond and the PND-derived magnetic easy axis of **1** is 31(6)°. The fact that such a tilt is observed, however, is a direct experimental confirmation of the *ab initio* result, which also shows this surprising tilting in the directions of the eigenaxes of the *D* tensor (*vide infra*). Intriguingly, the tilt away from the pseudo-C_4 axis makes the magnetic easy axis point more toward the pseudo-C_3 axis of the ideal octahedron. Previously, PND studies on compounds with pseudo-octahedral molecular geometries showed that, for a Co(II) and a Fe(II) compound, the magnetic easy axis tends to align with a pseudo-C_3 axis rather than the pseudo-C_4 axis of the coordinating polyhedron.[87]

Alternating current (ac) magnetic susceptibility studies

Given the large easy-axis D of **1**, we investigated the magnetization relaxation dynamics of a polycrystalline sample of **1** in the presence of an oscillating ac field of 3 Oe in the absence and presence of an optimum external magnetic field. Surprisingly, in both cases, **1** does not show any out-of-phase susceptibility signals. This implies that QTM is the dominant relaxation pathway over thermally assisted relaxation mechanisms. Significant rhombicity (|E/D|) is introduced within **1**, presumably because of its low symmetry. In **1**, non-zero intermolecular antiferromagnetic exchange coupling is presumably mediated through H-bonding. Such supramolecular interactions, as well as dipolar interactions and possible hyperfine interactions, are likely to trigger reversal of the magnetization vector through under barrier mechanisms in the ground state m_s level. At this point, we would like to emphasize that the present work is not focused on investigation of the slow relaxation of magnetization behavior in **1**. Instead, the focus is to prove that we can stabilize an easy axis of D in the thermodynamically stable, routinely observed six-coordinate Co(II) ion exclusively through ligand choice. Studies of how to quench the unwanted relaxation mechanisms by other means are left for the future.

Theoretical investigations

To shed light on the origin of axial anisotropy in **1** and to rationalize the absence of slow relaxation of magnetization behavior despite the presence of large easy-axis D, we performed *ab initio* calculations based on the complete active space self-consistent field (CASSCF)/n-electron valence state perturbation theory (NEVPT2) methods using the ORCA 4.1.2 suite[88] and the coordinates obtained from unpolarized

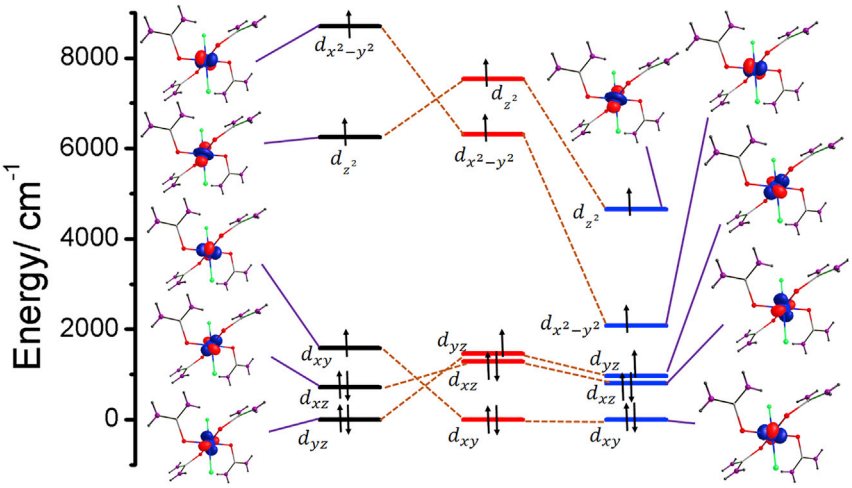

Figure 5. The eigenvalue plot of complex ND1 and the model complexes

A comparison of NEVPT2 AILFT orbital energies for **1b** (black trace), ND**1** (red trace), and **1c** (blue trace).

neutron diffraction, which is designated as ND1 (Supplemental experimental procedures). Only a marginal difference was noticed in SH parameters when carrying out the calculations on the coordinates derived from single-crystal X-ray diffraction of **1** (data not shown). Careful analysis of the structure reveals that the overall symmetry of the molecule is C_i and that the obtained ground state wave function is multideterminantal. The molecule was oriented so that the z axis pointed along with the Co-Cl bond and the x- and y-axes along with the Co-S bonds as much as possible.

The NEVPT2-computed SH parameters ($D = -84.1\ cm^{-1}$, $g_x = 2.00$, $g_y = 2.26$, $g_z = 3.06$, and $|E/D| = 0.22$) were used to simulate the experimental magnetic data. A good agreement between the simulated and the experimental data implies reliability of the computed parameters (Figure S3).[89] A measure of the rhombicity of the magnetic properties of this complex can be extracted similarly from PND measurements ($|E/D| = 0.25$), which is in good agreement with the computed $|E/D|$ of 0.22. The computed D value for ND**1** is overestimated slightly compared with the parameters extracted from the magnetic data fit.[77,90] Additionally, calculations performed using MOLCAS Suite 8.0 yielded a similar magnitude of D, offering confidence regarding the estimated values (see Tables S5 and S6 for details). Hence, we will discuss the parameters computed from NEVPT2 calculations in the following section. Despite a slight difference in D values, calculations and magnetic data fitting reveal an axial type anisotropy in **1** with significant rhombicity ($|E/D| = (0.22)$, which was confirmed unambiguously by PND measurements. The calculation gives a D_{zz} direction similar to what is observed in the PND measurement, with a 21.3° tilt with respect to the Co-Cl axis of ND**1** (Figure 1).

Next, we turned our attention to rationalize the origin of negative D observed in **1** using *ab initio* ligand field theory (AILFT) computed from the NEVPT2 wave function as implemented in ORCA 4.1.2.[88] The energy of the metal d orbitals for ND**1** is plotted in Figure 5, center panel, and follows the order of $d_{xy} < d_{xz} \sim d_{yz} < d_{x^2-y^2} < d_{z^2}$ (Table S7). The AILFT analysis reveal mixing of d orbitals as expected for a multideterminantal wave function from the CASSCF calculation (Table S7). It is well established that the spin-conserved transition between the orbitals having the same $|m_l|$ values (i.e., $d_{xz} \rightarrow d_{yz}$ and/or $d_{xy} \rightarrow d_{x^2-y^2}$) contributes to a negative D value, whereas

the transition between the orbitals of two different $|m_l|$ values contributes to positive values of D for the overall D of the complex.[29,34–37,46,49,67,91] For the computed overall D of ND**1**, the first three transitions from S wave function to the excited-state wave functions contribute predominantly (Table S8). The lowest-energy transition is observed between the d_{xz} and d_{yz} orbitals, whereas the second and third transition is between d_{xy} and d_{yz} and d_{xz} and $d_{x^2-y^2}$, respectively (Figure 5). Because there is no change in $|m_l|$ value of the lowest-energy transition, it contributes to negative D, whereas the second and third transitions make a positive contribution to the overall computed D value.[40,43] The magnitude of the D contribution originating from the lowest-energy transition is significantly larger than the second and third transitions, and therefore **1** is stabilized with an axial anisotropy. This is in excellent agreement with the DC magnetic studies and PND investigations.

We also noticed that subtle variations in the structural parameters affect the computed SH parameters. For example, as mentioned above in the structural description of **1** or ND**1**, the S-Co-S bond angles are not exactly 90° (∠S1-Co1-S2 = 87.8°, ∠S1-Co-S2# = 92.2°). To examine the effect of geometrical distortion in the equatorial plane of the Co(II) ion on the magnetic properties, we performed calculations on a model complex (**1a**) derived from ND**1**. This model complex (**1a**) has all S-Co-S angles at 90°, whereas the rest of the structural parameters were unchanged. The calculations performed on model **1a** reveals the following changes (Figure S4). (1) The overall D value of **1a** was found to increase by ∼12 cm^{-1} (Table S8) and the d orbital ordering trend of **1a** is similar to that of ND**1**, as expected. (2) The overall d orbital splitting energy of **1a** is slightly higher than ND**1**. (3) The energy of d_{xz} is unchanged in ND**1** and **1a**, whereas the d_{yz} orbital is slightly lower in energy in **1a** compared with ND**1**; i.e., a smaller energy gap between the d_{xz} and d_{yz} orbitals in **1a** compared with ND**1** (164 and 177 cm^{-1} for **1a** and ND**1**, respectively). Because of this, the lowest-energy transition contribution to the overall D is increased by ∼12 cm^{-1}, and this rationalizes the overall D enhancement in **1a** compared with ND**1** (Table S8). (4) In contrast, the energy of the $d_{x^2-y^2}$ and d_z^2 orbitals in **1a** is increased slightly compared with ND**1**. This is attributed to the increased M-L σ-bonding strength in **1a** compared with ND**1**. Second-order perturbation theory analysis from natural bond orbital (NBO) calculations performed on **1** and **1a** is consistent with this observation, where the M-L σ-bonding strength is relatively higher in **1a** than in **1** (Figure S5), and the D_{zz} of ND**1a** (22.7° from the Co-Cl axis) deviates slightly from ND**1**. Similarly, upon changing the Co-Cl and Co-S bond lengths, a significant change in D value is observed (*vide infra*).

Influence of hard donor versus soft donor on D

To understand, how soft donors, such as sulfur, play an important role in controlling the D value in complex ND**1**, we performed calculations on another model complex with the molecular formula $[Co(L_2)_4(Cl)_2]$ (**1b**; where L_2 = NH_2-CO-NH_2 [urea]), which is again derived from ND**1** by keeping all other structural parameters constant except the Co-O distance of the urea ligand (L_2). The Co-O distance was kept at 2.100 Å in **1b**, which is based on the distance observed for the other Co^{II}-urea metal complexes reported in the literature.[92,93] Such structural arrangement results in axially elongated geometry for Co(II) in **1b** (Co-Cl_{axial} = 2.461 Å and Co-$O_{equatorial}$ = 2.100 Å), in contrast to the geometry observed in ND**1**. The calculations performed on **1b** reveal that (1) the sign of the overall D value changes from negative to positive D (+43.7 cm^{-1}, |E/D| = 0.14) in **1b** compared with ND**1**, and (2) the d orbital ordering in **1b** is found to be $d_{yz} < d_{xz} < d_{xy} < d_z^2 < d_{x^2-y^2}$ (Figure 5). Like in **1b**, many Co(II) complexes reported in the literature possess elongated octahedral geometry, and these are expected to yield positive D values. To reaffirm this point, we performed

calculations on the X-ray structure of $[Co(pyridine)_4(Cl)_2]$ (2; Cambridge Crystallographic Data Center [CCDC] number 813722 and CSD code GOKGIY), where the Co(II) ion possess axially elongated geometry. As predicted, the computed D value is found to be positive for 2 (+124 cm^{-1}; Figure S6). Similarly, Travincek and coworkers reported another axially elongated Co(II) complex ($[Co(abpt)_2(tcm)_2]$, 3; CCDC number 997721 and CSD code EQINID) with a positive D (+48 cm^{-1}), which is rationalized elegantly by theoretical calculations.[94] A thorough literature search reveals several examples of axially elongated Co(II) octahedrals with various donor atoms, such as CoO_6, CoN_6, CoN_4O_2, CoN_2O_4, and CoN_3O_3, and all of these examples registered with a positive D (in the range of 18.6–117 cm^{-1}).

The overall positive D computed for model **1b** can be envisaged easily from the lowest-energy transition, and these are $d_{xz} \rightarrow d_{xy}$ or $d_{yz} \rightarrow d_{xy}$, both involving a change in |ml| value. In general, the first-row transition metal ions favor strong σ donor atoms, such as oxygen or nitrogen; hence, the metal-ligand bond distance (O or N) will be shorter than the M-X (X = halides) distance. Therefore, by swapping the soft donor ligands in ND**1** with hard donor ligands, such as urea, significantly changes the electronic structure of the Co(II) ion in its distorted octahedral environment.

Influence of donor atoms versus geometry on the D of Co(II) complexes

To address whether geometry plays a major role or whether the coordinated atoms possess a non-zero influence on the D of the octahedral Co(II) complexes, we created another model complex, **1c**, from ND**1**, where we replaced the S donor atoms with oxygen (simply, thiourea to urea) and kept all other structural parameters constant; i.e., the Co-O bond distance was kept constant as in Co-S (2.501(5) and 2.548(6)). This is an unrealistic model used only for the purpose of understanding the role of substitution. In reality, Co-O bond distances are typically in the range of 2.08–2.19 Å.[33,64,67] Calculations on this model are performed purely to understand the nature of donor atom influence compared with the geometry on sign and magnitude of D. In these **1c** model complex calculations, we observed the following changes compared with ND**1**. (1) The negative sign of D is maintained as in ND**1**, and, more importantly, the magnitude of D increased by an approximate factor of two (−151.6 cm^{-1} and |E/D| = 0.16; Table S8). (2) As expected, the orbital ordering follows the same trend as in ND**1**; nevertheless, the overall d orbital splitting is reduced drastically, nearly by a factor of two, as shown in Figure 5. Because of this, the energy gap between the orbitals involved in the lowest-energy transition (d_{xz} and d_{yz}) is reduced by a factor of ∼3 in **1c** (64 cm^{-1}) compared with ND**1** (177.4 cm^{-1}). Consequently, the lowest-energy transition contribution to the overall D value of **1c** increases drastically compared with ND**1** and, therefore, rationalizes the nearly 2-fold rise in overall D value in **1c** compared with ND**1**.

The calculations performed on ND**1** and the various model complexes unveil that maintaining the axially compressed geometry around Co(II) is the predominant factor (irrespective of any donor atoms) that stabilizes the large axial D. Despite a large axial anisotropy registered in **1**, the absence of slow relaxation of magnetization is attributed to the reduction in overall symmetry of the molecule, resulting in increased rhombicity. This facilitates heavy mixing of the S wave function with an excited-state wave function, triggering fast relaxation and rationalizing the absence of out-of-phase susceptibility signals in **1**. Therefore, the ligand that enforces higher-order symmetry around Co(II) is likely to stabilize not only large negative D but also yield smaller |E/D|, a perfect combination to realize SIM behavior. However, stabilizing an axially compressed geometry with hard donors, such as oxygen or nitrogen,

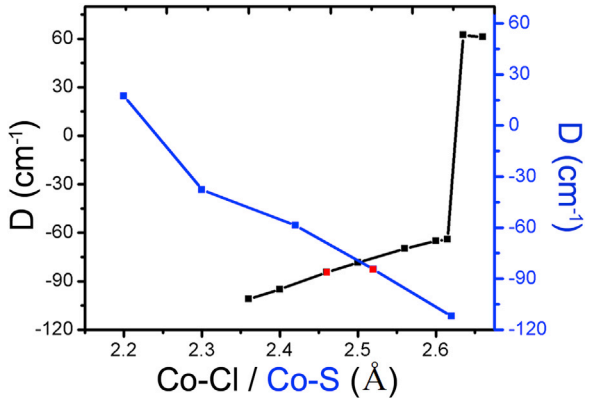

Figure 6. Magnetostructural correlation developed for 1

Co-Cl distances are varied while keeping Co-S distance constant and vice versa. Shown is the variation observed in the absolute value of D as a function of Co-Cl (black) and Co-S (blue trace) bond distance. The red data point indicates the actual Co-Cl and Co-S bond distance observed in ND**1**.

is an extremely difficult task (as evidenced by the literature showing that an axially elongated geometry is favored over the axially compressed one with hard donor atoms). On the other hand, realizing an axially compressed geometry with more diffuse and soft donor ligands, such as sulfur (or ≥ 3p valence ligand), is a fruitful synthetic strategy to realize easy-axis D in six-coordinate Co(II) complexes in a targeted approach.

Magnetostructural correlation studies

To assist the synthetic chemist to rationally target ligands that can stabilize large negative D, we performed magnetostructural correlations by systematically varying the Co-Cl distance from 2.35 to 2.65 Å while keeping Co-S distance constant and vice versa (the Co-S bond distance varies from 2.2–2.6 Å) in ND**1**.

Although the various models generated from ND**1** could be unrealistic, this serves the purpose of assessing the role of individual structural parameters in controlling the D values. These sets of calculations unveil that, if the Co-Cl distance is smaller than the Co-S distance (i.e., an axially compressed octahedral geometry), then large negative D is stabilized. When the Co-Cl bond distance exceeds the Co-S bond distance (i.e., axially elongated geometry), the sign of D is reversed; i.e., positive (Figure 6). Similar observations have been obtained using high-pressure crystallography combined with theoretical calculations on Co(II) complexes.[95] The calculations predict that strong axial bonds and weak equatorial bonds (i.e., axially compressed octahedral geometry) is the best combination to stabilize the large axial anisotropy in air-stable Co(II) six-coordinate complexes. In line with this strategy, we attempted to replace the axial $–Cl^{-}$ ligand in **1** by $–F^{-}$ using anhydrous CoF_2 salt; however, this resulted in a tetrahedral $[Co(L_1)_4]SiF_6$ complex.[51] We succeeded in reducing the Co-axial distance by ~0.44 Å when $Co(NCS)_2$ was used instead of anhydrous CoF_2 or $CoCl_2.6H_2O$. But, unexpectedly, we isolated a 1D chain with the molecular formula of $[Co(\mu\text{-}L_1)_2(NCS)_2]_n$ rather than a discrete octahedral Co(II) complex. Preliminary data collected suggest that our predictions are indeed valid, and a thorough study of this molecule will be reported elsewhere. Preliminary results show an isolated 1D $[Co(tu)_2(NCS)_2]_n$ chain, and, according to our prediction, the axial bond distance Co-N (2.0157 A) is reduced by 0.4455 A compared with **1**, whereas a marginal change in Co-S distance is observed between **1** and the 1D chain. As a consequence,

the computed D (−115.07 cm^{-1}) (E/D [0.18]) in the 1D chain is increased, and the D_{zz} tends to move toward the Co-Cl axis (the deviation of D_{zz} from Co-Cl is 14.15°, unlike the scenario observed in **1** or ND**1**. On the other hand, a two-coordinate Co(II) complex reported by Yao et al.[28] elegantly established that the molecule behaves as an excellent single-molecule magnet with one of the largest energy barriers (413 cm^{-1}) known for a monomeric transition metal complex reported in the literature. Although the two-coordinate complexes shed light on the mechanism of relaxation, realization of molecule-based devices with extremely reactive complexes is challenging. Hence, it is imperative to stabilize a large negative D value in the air-stable complex to aid device fabrication.

We discovered the key to unlock the mystery of stabilizing the easy axis of D in six-coordinate Co(II) complexes in a targeted manner for the first time. Lack of such systematic investigation in the literature presumably compounded the inability of conventional methods, such as electron paramagnetic resonance, to determine the sign and magnitude of D because $h\nu << D$. The reported complex, **1**, not only overcomes the long-standing issue (i.e., stabilization with a negative D value [−63(10) cm^{-1}]) but also unravels the parameters that control the sign and magnitude of the D value of the Co(II) distorted octahedral complex, which is unprecedented. We employed a sophisticated analytical technique (PND methods) to determine the axial anisotropy associated with **1**, which is firmly supported by the magnetic data. The electronic structure and easy axis D of **1** are rationalized by detailed theoretical calculations that also suggest that the |E/D| value is significantly large, diminishing the prospect of magnetic blocking. The SH parameters extracted are in good agreement with the magnetic data and PND measurements. Therefore, the finding reported here will pave the way for the synthetic chemist to realize a new generation of air-stable, thermodynamically favorable, six-coordinate Co(II) complexes with an easy axis of magnetization coupled with improved T_B in a targeted manner. This will eventually make molecularly based information storage devices a reality.

EXPERIMENTAL PROCEDURES

Resource availability

Lead contact

Further information and requests for resources should be directed to and will be fulfilled by the lead contact, Maheswaran Shanmugam (eswar@chem.iitb.ac.in).

Materials availability

This study did not generate new unique reagents.

Data and code availability

Crystal data for **1** are available from the Cambridge Crystallographic Data Centre under CSD code CTHUCO10. The computational output is available from the authors upon request.

Synthesis

All reactions were carried out under aerobic conditions unless otherwise mentioned. All chemicals and solvents were purchased from commercially available sources (Alfa Aesar or Sigma-Aldrich) and used without any further purification. Elemental analysis was carried out with a Thermo Finnigan device. The magnetic data were collected on an MPMS-XL SQUID magnetometer equipped with a 7-kOe superconducting magnet in the temperature range of 2−300 K. Single-crystal X-ray diffraction for complex **1** was performed on a Rigaku Saturn charge-coupled device (CCD) diffractometer using a graphite monochromator (λ = 0.71073 Å). Unit cell determination and

data reduction were performed using CrysAlisPro 1.171.38.43 (Rigaku OD).[96] With the help of SHELXL-2014/7,[97] the structures were solved by direct methods and refined by least-squares procedures on F^2. All non-hydrogen atoms were refined anisotropically, and hydrogen atoms were refined using a riding model.

The thiourea ligand (L_1, 1.0 g, 13.1 mmol) was added to the warm (35°C–40°C) ethanolic solution of $CoCl_2.6H_2O$ (0.778 g, 3.2 mmol). The reaction mixture was heated under reflux for 6 h and then allowed to cool to room temperature. The solution was removed under reduced pressure, and the obtained residue was dissolved in ethyl acetate (~3–4 mL). Blue block-shaped crystals of **1**, suitable for X-ray diffraction, were grown after 7 days from filtrate upon slow evaporation at room temperature (yield [based on Co(II)], 0.87 g [58%]; elemental analysis: calculated: C, 11.06; H, 3.71; N, 25.79; found: C, 10.92; H, 3.71; N, 25.28).

The bulk phase purity of complex **1** was checked by powder X-ray diffraction (PXRD). The experimental PXRD data of **1** are in good agreement with the simulated data derived from its corresponding single-crystal data (Figure S7).

DC magnetization measurements

DC magnetization measurements were performed using a physical property measurement system (PPMS) VSM magnetometer as well as an magnetic property measurement system (MPMS) magnetometer from Quantum Design equipped with a 14-T and 7-T magnet, respectively. Pulsed magnetic field magnetization was measured up to 555 kOe at the High Magnetic Field Laboratory Dresden by an induction method using a coaxial pick-up coil system.[98] The total pulse duration time was 25 ms. Because of the short rise time of only 7 ms, the up-sweep data showed a significant influence of hysteretic effects, which is why only the data obtained during the much slower down sweep were used for evaluation. The pulsed magnetic field magnetization data were calibrated to the static magnetic field measurement (Figure 3, inset). Simulation of the data was done using the EasySpin software package[90] as well a QMC method with the stochastic series expansion algorithm as implemented in the Algorithms and Libraries for Physics Simulations (ALPS) software package.[99,100]

Polarized neutron diffraction

The D of molecular complexes can be asserted by measuring so-called site susceptibilities for all magnetic ions in the structure.[101] The method uses magnetic scattering from a magnetized sample, which can be modeled through the standard expression for the magnetic structure factors,

$$F_M(\mathbf{Q}) = \sum_i f_i \boldsymbol{m}_i e^{-i\mathbf{Q}\cdot\boldsymbol{r}_i} e^{-W_i}$$

where $\mathbf{Q}$ is the scattering vector and f_i, $\boldsymbol{m}_i$, $\boldsymbol{r}_i$, and W_i are the magnetic form factor, magnetic moment, position, and Debye-Waller factor of the i^{th} atom, respectively. Instead of modeling the magnetic moment directly, however, the method of site susceptibilities introduces an atomic susceptibility tensor through the equation

$$\boldsymbol{m}_i = \underline{\underline{\boldsymbol{\chi}}}_i H$$

where H is an externally applied field. The magnetic structure factor can then be rewritten to give

$$F_M(\mathbf{Q}) = \sum_{i,j} \frac{1}{N_{i,j}} \boldsymbol{R}_j \boldsymbol{\chi}_i \boldsymbol{R}_j^{-1} e^{-i\mathbf{Q}\cdot\left(\boldsymbol{R}_j \boldsymbol{r}_i + \boldsymbol{t}_j\right)} \cdot H$$

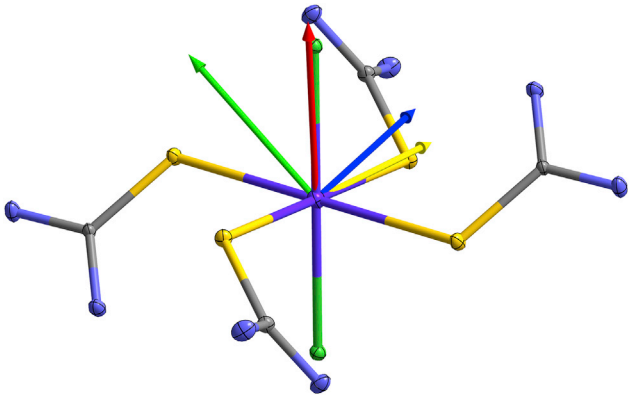

Figure 7. Molecular structure of 1 as determined from unpolarized neutron diffraction (50% probability)

Shown are the vectors describing the direction of the magnetic fields applied for the polarized diffraction measurements. Red, blue, green, and yellow arrows represent orientations 1, 2, 3, and 4, respectively (refer to Table S2 for details).

Here, $\boldsymbol{R}_j$ and $\boldsymbol{t}_j$ are the symmetry operators that are applied to the i^{th} atom. Determination of the six independent susceptibility tensor components requires multiple directions of the applied field.

This gives direct experimental access to the type of D and the direction of the main magnetic axes of a given compound. Furthermore, using polarized neutrons allows definition of a flipping ratio,[102] whose use increases the experimental sensitivity to the magnetic scattering that is comparatively weak for crystals of paramagnetic complexes. We have used this technique previously to elucidate the D of Dy(III)-based SIMs,[103] and others have used it similarly on a range of SIMs containing transition metal ions.[87,104–106] Single-crystal polarized neutron scattering data for **1** were combined from measurements at the beamline HB3A situated on the igh-flux isotope reactor (HFIR) at Oak Ridge National Laboratory (ORNL)[107] and at the 6T2 diffractometer of the Laboratorie Leon Brillouin (LLB).[108] The HB3A diffractometer employs a supermirror to polarize the incident neutrons. By using a Heusler alloy analyzer crystal, the beam polarization was measured prior to the experiment to be 94%. A magnetic field of 7.8 kOe was applied at the position of the crystal with a set of permanent magnets attached to the sample holder. At this field strength, magnetization is within the linear range with respect to the applied field (Figure 3). For the experiment, a single crystal with dimensions of 3 × 1.8 × 1.5 mm^3 was glued to an aluminum pin, and the crystal was centered in the beam.

Diffracted intensities were measured at a temperature of 6 K for two different directions of the applied field with respect to the crystal. Bragg peaks were moved into diffraction conditions and kept at a fixed setting of the diffractometer angles while measuring for 300 s. Intensities were extracted from the frames using a Python script developed in collaboration with the beamline staff, and the flipping ratios and associated uncertainties were calculated based on this intensity extraction. On 6T2, the supermirror gives a beam polarization of 0.905 at an applied field of 10 kOe. The same crystal as measured on HB3A was used. Flipping ratios were extracted from the diffraction data using the LLB in-house program suite. Details regarding the collected flipping ratio data are summarized in Table S2. The magnetic field directions in Table S2 were plotted on top of the molecule that is constructed when considering the effect of inversion symmetry on the asymmetric unit Figure 7.

Single-crystal non-polarized neutron diffraction

Unpolarized single-crystal neutron diffraction was measured on a single crystal of **1** on the KOALA diffractometer of the Australian Centre for Neutron Scattering (ACNS).[109]

The crystal structure was refined using SHELXL[92] through the Olex2-interface[110] with the previously determined X-ray structure as a starting model. The model was refined against the neutron diffraction data without constraints on the hydrogen atoms so that thermal vibrations and positions were freely refined. Diffraction using the Laue technique with $(\sin\theta_{max}/\lambda) = 0.84$ Å^{-1} gave 5,373 unique reflections used for refinement of the nuclear structure (Table 1).

SUPPLEMENTAL INFORMATION

Supplemental information can be found online at https://doi.org/10.1016/j.xcrp.2021.100404.

ACKNOWLEDGMENTS

M.S. thanks SERB (CRG/2019/004185 and SPR/2019/001145), CSIR (01(2933)/18/EMR-II), and IIT Bombay for financial assistance. G.R. thanks SERB for funding (CRG/2018/000430, DST/SJF/CSA-03/2018-10, and SB/SJF/2019-20/12). J.O. and E.A.K. thank the Danish National Research Foundation (DNRF-93) and the Villum Foundation for financial support. Affiliation with the Center for Integrated Materials Research (iMAT) at Aarhus University is gratefully acknowledged (J.O.).The authors gratefully acknowledge the beamtime at the high-flux isotope reactor (HFIR) and Laboratoire Leon-Brillouin. Bryan C. Chakoumakos provided logistical support for the experiments at the HFIR. A portion of this research used resources at the HFIR, a DOE Office of Science User Facility operated by the Oak Ridge National Laboratory. This work is supported by the Deutsche Forschungsgemeinschaft (DFG; German Research Foundation) under Germany's Excellence Strategy EXC2181/1-390900948 (the Heidelberg STRUCTURES Excellence Cluster), by the BMBF via the SpinFun project (13XP5088), and by the HLD at HZDR, a member of the European Magnetic Field Laboratory (EMFL). We thank Dr. Marc Uhlarz for technical support during the pulsed-field magnetization measurements.

AUTHOR CONTRIBUTIONS

S.T. and S.V. synthesized and characterized the compounds and modeled magnetic data. S.T. performed the computational calculations. N.A. performed MOLCAS calculations under the supervision of G.R. E.A.K. performed PND measurements with H.C. under the supervision of J.O. L.S. performed static field magnetization measurements and performed QMC simulations under the supervision of C.K. and R.K. S.S. performed pulsed-field magnetization measurements supervised by R.K. M.S. designed and supervised the work. All authors contributed to writing the manuscript.

DECLARATION OF INTERESTS

The authors declare no competing interests.

Received: June 22, 2020
Revised: January 28, 2021
Accepted: March 19, 2021
Published: April 12, 2021

REFERENCES

1. Sessoli, R., Gatteschi, D., Caneschi, A., and Novak, M.A. (1993). Magnetic bistability in a metal-ion cluster. Nature *365*, 141–143.
2. Caneschi, A., Gatteschi, D., Sessoli, R., Barra, A.L., Brunel, L.C., and Guillot, M. (1991). Alternating current susceptibility, high field magnetization, and millimeter band EPR evidence for a ground S = 10 state in [Mn12O12(Ch3COO)16(H2O) 4].2CH3COOH.4H2O. J. Am. Chem. Soc. *113*, 5873–5874.
3. Gatteschi, D., Caneschi, A., Pardi, L., and Sessoli, R. (1994). Large clusters of metal ions: the transition from molecular to bulk magnets. Science *265*, 1054–1058.
4. Frost, J.M., Harriman, K.L.M., and Murugesu, M. (2016). The rise of 3-d single-ion magnets in molecular magnetism: towards materials from molecules? Chem. Sci. (Camb.) *7*, 2470–2491.
5. Chang, B., Wang, Q., Xie, H., and Liang, J.Q. (2011). Macroscopic quantum coherence in a single molecular magnet and Kondo effect of electron transport. Phys. Lett. A *375*, 2932–2938.
6. Schlegel, C., van Slageren, J., Manoli, M., Brechin, E.K., and Dressel, M. (2008). Direct observation of quantum coherence in single-molecule magnets. Phys. Rev. Lett. *101*, 147203.
7. Yang, J., Wang, Y., Wang, Z., Rong, X., Duan, C.-K., Su, J.-H., and Du, J. (2012). Observing quantum oscillation of ground states in single molecular magnet. Phys. Rev. Lett. *108*, 230501.
8. Clérac, R., and Winpenny, R.E.P. (2017). Single-Molecule Magnets and Related Phenomena. In 50 Years of Structure and Bonding, D.M.P. Mingos, ed. (Springer), pp. 35–48.
9. Bogani, L., and Wernsdorfer, W. (2008). Molecular spintronics using single-molecule magnets. Nat. Mater. *7*, 179–186.
10. Jenkins, M., Hümmer, T., Martínez-Pérez, M.J., García-Ripoll, J., Zueco, D., and Luis, F. (2013). Coupling single-molecule magnets to quantum circuits. New J. Phys. *15*, 095007.
11. Lehmann, J., Gaita-Arino, A., Coronado, E., and Loss, D. (2007). Spin qubits with electrically gated polyoxometalate molecules. Nat. Nanotechnol. *2*, 312–317.
12. Leuenberger, M.N., and Loss, D. (2001). Quantum computing in molecular magnets. Nature *410*, 789–793.
13. Long, D.-L., Burkholder, E., and Cronin, L. (2007). Polyoxometalate clusters, nanostructures and materials: from self assembly to designer materials and devices. Chem. Soc. Rev. *36*, 105–121.
14. Murrie, M. (2010). Cobalt(II) single-molecule magnets. Chem. Soc. Rev. *39*, 1986–1995.
15. Hoshino, N., Ako, A.M., Powell, A.K., and Oshio, H. (2009). Molecular magnets containing wheel motifs. Inorg. Chem. *48*, 3396–3407.
16. Meng, Y.-S., Jiang, S.-D., Wang, B.-W., and Gao, S. (2016). Understanding the Magnetic Anisotropy toward Single-Ion Magnets. Acc. Chem. Res. *49*, 2381–2389.
17. Milios, C.J., Inglis, R., Bagai, R., Wernsdorfer, W., Collins, A., Moggach, S., Parsons, S., Perlepes, S.P., Christou, G., and Brechin, E.K. (2007). Enhancing SMM properties in a family of [Mn6] clusters. Chem. Commun. (Camb.) (33), 3476–3478.
18. Neese, F., and Pantazis, D.A. (2011). What is not required to make a single molecule magnet. Faraday Discuss. *148*, 229–238, discussion 299–314.
19. Waldmann, O. (2007). A criterion for the anisotropy barrier in single-molecule magnets. Inorg. Chem. *46*, 10035–10037.
20. Ako, A.M., Hewitt, I.J., Mereacre, V., Clérac, R., Wernsdorfer, W., Anson, C.E., and Powell, A.K. (2006). A ferromagnetically coupled mn(19) aggregate with a record S=83/2 ground spin state. Angew. Chem. Int. Ed. Engl. *45*, 4926–4929.
21. Baniodeh, A., Magnani, N., Lan, Y., Buth, G., Anson, C.E., Richter, J., Affronte, M., Schnack, J., and Powell, A.K. (2018). High spin cycles: topping the spin record for a single molecule verging on quantum criticality. npj Quantum Mater. *3*, 1–6.
22. Chen, W.-P., Singleton, J., Qin, L., Camón, A., Engelhardt, L., Luis, F., Winpenny, R.E.P., and Zheng, Y.-Z. (2018). Quantum Monte Carlo simulations of a giant $Ni_{21}Gd_{20}$ cage with a S = 91 spin ground state. Nat. Commun. *9*, 2107.
23. Kang, S., Zheng, H., Liu, T., Hamachi, K., Kanegawa, S., Sugimoto, K., Shiota, Y., Hayami, S., Mito, M., Nakamura, T., et al. (2015). A ferromagnetically coupled Fe42 cyanide-bridged nanocage. Nat. Commun. *6*, 5955.
24. Milios, C.J., Inglis, R., Vinslava, A., Bagai, R., Wernsdorfer, W., Parsons, S., Perlepes, S.P., Christou, G., and Brechin, E.K. (2007). Toward a magnetostructural correlation for a family of Mn6 SMMs. J. Am. Chem. Soc. *129*, 12505–12511.
25. Harman, W.H., Harris, T.D., Freedman, D.E., Fong, H., Chang, A., Rinehart, J.D., Ozarowski, A., Sougrati, M.T., Grandjean, F., Long, G.J., et al. (2010). Slow magnetic relaxation in a family of trigonal pyramidal iron(II) pyrrolide complexes. J. Am. Chem. Soc. *132*, 18115–18126.
26. Bunting, P.C., Atanasov, M., Damgaard-Møller, E., Perfetti, M., Crassee, I., Orlita, M., Overgaard, J., van Slageren, J., Neese, F., and Long, J.R. (2018). A linear cobalt(II) complex with maximal orbital angular momentum from a non-Aufbau ground state. Science *362*, eaat7319.
27. Poulten, R.C., Page, M.J., Algarra, A.G., Le Roy, J.J., López, I., Carter, E., Llobet, A., Macgregor, S.A., Mahon, M.F., Murphy, D.M., et al. (2013). Synthesis, electronic structure, and magnetism of [Ni(6-Mes)2]+: a two-coordinate nickel(I) complex stabilized by bulky N-heterocyclic carbenes. J. Am. Chem. Soc. *135*, 13640–13643.
28. Yao, X.-N., Du, J.-Z., Zhang, Y.-Q., Leng, X.-B., Yang, M.-W., Jiang, S.-D., Wang, Z.-X., Ouyang, Z.-W., Deng, L., Wang, B.-W., and Gao, S. (2017). Two-Coordinate Co(II) Imido Complexes as Outstanding Single-Molecule Magnets. J. Am. Chem. Soc. *139*, 373–380.
29. Zadrozny, J.M., Atanasov, M., Bryan, A.M., Lin, C.-Y., Rekken, B.D., Power, P.P., Neese, F., and Long, J.R. (2013). Slow magnetization dynamics in a series of two-coordinate iron(ii) complexes. Chem. Sci. (Camb.) *4*, 125–138.
30. Zadrozny, J.M., Xiao, D.J., Atanasov, M., Long, G.J., Grandjean, F., Neese, F., and Long, J.R. (2013). Magnetic blocking in a linear iron(I) complex. Nat. Chem. *5*, 577–581.
31. Herchel, R., Váhovská, L., Potočňák, I., and Trávníček, Z. (2014). Slow magnetic relaxation in octahedral cobalt(II) field-induced single-ion magnet with positive axial and large rhombic anisotropy. Inorg. Chem. *53*, 5896–5898.
32. Rechkemmer, Y., Breitgoff, F.D., van der Meer, M., Atanasov, M., Hakl, M., Orlita, M., Neugebauer, P., Neese, F., Sarkar, B., and van Slageren, J. (2016). A four-coordinate cobalt(II) single-ion magnet with coercivity and a very high energy barrier. Nat. Commun. *7*, 10467.
33. Roy, S., Oyarzabal, I., Vallejo, J., Cano, J., Colacio, E., Bauza, A., Frontera, A., Kirillov, A.M., Drew, M.G.B., and Das, S. (2016). Two Polymorphic Forms of a Six-Coordinate Mononuclear Cobalt(II) Complex with Easy-Plane Anisotropy: Structural Features, Theoretical Calculations, and Field-Induced Slow Relaxation of the Magnetization. Inorg. Chem. *55*, 8502–8513.
34. Vaidya, S., Shukla, P., Tripathi, S., Rivière, E., Mallah, T., Rajaraman, G., and Shanmugam, M. (2018). Substituted versus Naked Thiourea Ligand Containing Pseudotetrahedral Cobalt(II) Complexes: A Comparative Study on Its Magnetization Relaxation Dynamics Phenomenon. Inorg. Chem. *57*, 3371–3386.
35. Vaidya, S., Tewary, S., Singh, S.K., Langley, S.K., Murray, K.S., Lan, Y., Wernsdorfer, W., Rajaraman, G., and Shanmugam, M. (2016). What Controls the Sign and Magnitude of Magnetic Anisotropy in Tetrahedral Cobalt(II) Single-Ion Magnets? Inorg. Chem. *55*, 9564–9578.
36. Vaidya, S., Upadhyay, A., Singh, S.K., Gupta, T., Tewary, S., Langley, S.K., Walsh, J.P.S., Murray, K.S., Rajaraman, G., and Shanmugam, M. (2015). A synthetic strategy for switching the single ion anisotropy in tetrahedral Co(II) complexes. Chem. Commun. (Camb.) *51*, 3739–3742.
37. Zadrozny, J.M., Liu, J., Piro, N.A., Chang, C.J., Hill, S., and Long, J.R. (2012). Slow magnetic relaxation in a pseudotetrahedral cobalt(II) complex with easy-plane anisotropy. Chem. Commun. (Camb.) *48*, 3927–3929.
38. Boča, R. (2004). Zero-field splitting in metal complexes. Coord. Chem. Rev. *248*, 757–815.

39. Boca, R. (2006). Magnetic parameters and magnetic functions in mononuclear complexes beyond the spin-Hamiltonian formalism. Struct. Bonding *117*, 1–264.

40. Dai, D., Xiang, H., and Whangbo, M.-H. (2008). Effects of spin-orbit coupling on magnetic properties of discrete and extended magnetic systems. J. Comput. Chem. *29*, 2187–2209.

41. El-Khatib, F., Cahier, B., Shao, F., López-Jordà, M., Guillot, R., Rivière, E., Hafez, H., Saad, Z., Girerd, J.-J., Guihéry, N., and Mallah, T. (2017). Design and Magnetic Properties of a Mononuclear Co(II) Single Molecule Magnet and Its Antiferromagnetically Coupled Binuclear Derivative. Inorg. Chem. *56*, 4602–4609.

42. Ruamps, R., Batchelor, L.J., Guillot, R., Zakhia, G., Barra, A.-L., Wernsdorfer, W., Guihéry, N., and Mallah, T. (2014). Ising-type magnetic anisotropy and single molecule magnet behaviour in mononuclear trigonal bipyramidal Co(ii) complexes. Chem. Sci. (Camb.) *5*, 3418–3424.

43. Ruamps, R., Batchelor, L.J., Maurice, R., Gogoi, N., Jiménez-Lozano, P., Guihéry, N., de Graaf, C., Barra, A.-L., Sutter, J.-P., and Mallah, T. (2013). Origin of the magnetic anisotropy in heptacoordinate Ni(II) and Co(II) complexes. Chemistry *19*, 950–956.

44. Shao, F., Cahier, B., Guihéry, N., Rivière, E., Guillot, R., Barra, A.-L., Lan, Y., Wernsdorfer, W., Campbell, V.E., and Mallah, T. (2015). Tuning the Ising-type anisotropy in trigonal bipyramidal Co(II) complexes. Chem. Commun. (Camb.) *51*, 16475–16478.

45. Shao, F., Cahier, B., Rivière, E., Guillot, R., Guihéry, N., Campbell, V.E., and Mallah, T. (2017). Structural Dependence of the Ising-type Magnetic Anisotropy and of the Relaxation Time in Mononuclear Trigonal Bipyramidal Co(II) Single Molecule Magnets. Inorg. Chem. *56*, 1104–1111.

46. Suturina, E.A., Nehrkorn, J., Zadrozny, J.M., Liu, J., Atanasov, M., Weyhermüller, T., Maganas, D., Hill, S., Schnegg, A., Bill, E., et al. (2017). Magneto-Structural Correlations in Pseudotetrahedral Forms of the $[Co(SPh)_4]^{2-}$ Complex Probed by Magnetometry, MCD Spectroscopy, Advanced EPR Techniques, and ab Initio Electronic Structure Calculations. Inorg. Chem. *56*, 3102–3118.

47. Woods, T.J., Ballesteros-Rivas, M.F., Gómez-Coca, S., Ruiz, E., and Dunbar, K.R. (2016). Relaxation Dynamics of Identical Trigonal Bipyramidal Cobalt Molecules with Different Local Symmetries and Packing Arrangements: Magnetostructural Correlations and ab inito Calculations. J. Am. Chem. Soc. *138*, 16407–16416.

48. Wu, T., Zhai, Y.-Q., Deng, Y.-F., Chen, W.-P., Zhang, T., and Zheng, Y.-Z. (2019). Correlating magnetic anisotropy with the subtle coordination geometry variation of a series of cobalt(ii)-sulfonamide complexes. Dalton Trans. *48*, 15419–15426.

49. Zadrozny, J.M., and Long, J.R. (2011). Slow magnetic relaxation at zero field in the tetrahedral complex [Co(SPh)4]2-. J. Am. Chem. Soc. *133*, 20732–20734.

50. Zadrozny, J.M., Telser, J., and Long, J.R. (2013). Slow magnetic relaxation in the tetrahedral cobalt(II) complexes [Co(EPh)4]2– (EO, S, Se). Polyhedron *64*, 209–217.

51. Tripathi, S., Vaidya, S., Ansari, K.U., Ahmed, N., Rivière, E., Spillecke, L., Koo, C., Klingeler, R., Mallah, T., Rajaraman, G., and Shanmugam, M. (2019). Influence of a Counteranion on the Zero-Field Splitting of Tetrahedral Cobalt(II) Thiourea Complexes. Inorg. Chem. *58*, 9085–9100.

52. Zhu, Y.-Y., Zhang, Y.-Q., Yin, T.-T., Gao, C., Wang, B.-W., and Gao, S. (2015). A Family of Co(II)Co(III)3 Single-Ion Magnets with Zero-Field Slow Magnetic Relaxation: Fine Tuning of Energy Barrier by Remote Substituent and Counter Cation. Inorg. Chem. *54*, 5475–5486.

53. Jurca, T., Farghal, A., Lin, P.-H., Korobkov, I., Murugesu, M., and Richeson, D.S. (2011). Single-molecule magnet behavior with a single metal center enhanced through peripheral ligand modifications. J. Am. Chem. Soc. *133*, 15814–15817.

54. Rajnák, C., Titiš, J., Fuhr, O., Ruben, M., and Boča, R. (2014). Single-molecule magnetism in a pentacoordinate cobalt(II) complex supported by an antenna ligand. Inorg. Chem. *53*, 8200–8202.

55. Schweinfurth, D., Krzystek, J., Atanasov, M., Klein, J., Hohloch, S., Telser, J., Demeshko, S., Meyer, F., Neese, F., and Sarkar, B. (2017). Tuning Magnetic Anisotropy Through Ligand Substitution in Five-Coordinate Co(II) Complexes. Inorg. Chem. *56*, 5253–5265.

56. Cahier, B., Maurice, R., Bolvin, H., Mallah, T., and Guihéry, N. (2016). Tools for Predicting the Nature and Magnitude of Magnetic Anisotropy in Transition Metal Complexes: Application to Co(II) Complexes. Magnetochemistry *2*, 31.

57. Colacio, E., Ruiz, J., Ruiz, E., Cremades, E., Krzystek, J., Carretta, S., Cano, J., Guidi, T., Wernsdorfer, W., and Brechin, E.K. (2013). Slow magnetic relaxation in a Co(II)-Y(III) single-ion magnet with positive axial zero-field splitting. Angew. Chem. Int. Ed. Engl. *52*, 9130–9134.

58. Vallejo, J., Castro, I., Ruiz-García, R., Cano, J., Julve, M., Lloret, F., De Munno, G., Wernsdorfer, W., and Pardo, E. (2012). Field-induced slow magnetic relaxation in a six-coordinate mononuclear cobalt(II) complex with a positive anisotropy. J. Am. Chem. Soc. *134*, 15704–15707.

59. Novikov, V.V., Pavlov, A.A., Belov, A.S., Vologzhanina, A.V., Savitsky, A., and Voloshin, Y.Z. (2014). Transition Ion Strikes Back: Large Magnetic Susceptibility Anisotropy in Cobalt(II) Clathrochelates. J. Phys. Chem. Lett. *5*, 3799–3803.

60. Novikov, V.V., Pavlov, A.A., Nelyubina, Y.V., Boulon, M.-E., Varzatskii, O.A., Voloshin, Y.Z., and Winpenny, R.E.P. (2015). A Trigonal Prismatic Mononuclear Cobalt(II) Complex Showing Single-Molecule Magnet Behavior. J. Am. Chem. Soc. *137*, 9792–9795.

61. Pavlov, A.A., Nelyubina, Y.V., Kats, S.V., Penkova, L.V., Efimov, N.N., Dmitrienko, A.O., Vologzhanina, A.V., Belov, A.S., Voloshin, Y.Z., and Novikov, V.V. (2016). Polymorphism in a Cobalt-Based Single-Ion Magnet Tuning Its Barrier to Magnetization Relaxation. J. Phys. Chem. Lett. *7*, 4111–4116.

62. Pavlov, A.A., Savkina, S.A., Belov, A.S., Nelyubina, Y.V., Efimov, N.N., Voloshin, Y.Z., and Novikov, V.V. (2017). Trigonal Prismatic Tris-pyridineoximate Transition Metal Complexes: A Cobalt(II) Compound with High Magnetic Anisotropy. Inorg. Chem. *56*, 6943–6951.

63. Tripathi, S., Dey, A., Shanmugam, M., Narayanan, R.S., and Chandrasekhar, V. (2019). Cobalt(II) Complexes as Single-Ion Magnets. In Organometallic Magnets, V. Chandrasekhar and F. Pointillart, eds. (Springer), pp. 35–75.

64. Gómez-Coca, S., Urtizberea, A., Cremades, E., Alonso, P.J., Camón, A., Ruiz, E., and Luis, F. (2014). Origin of slow magnetic relaxation in Kramers ions with non-uniaxial anisotropy. Nat. Commun. *5*, 4300.

65. Deng, Y.-F., Singh, M.K., Gan, D., Xiao, T., Wang, Y., Liu, S., Wang, Z., Ouyang, Z., Zhang, Y.-Z., and Dunbar, K.R. (2020). Probing the Axial Distortion Effect on the Magnetic Anisotropy of Octahedral Co(II) Complexes. Inorg. Chem. *59*, 7622–7630.

66. Sato, R., Suzuki, K., Minato, T., Shinoe, M., Yamaguchi, K., and Mizuno, N. (2015). Field-induced slow magnetic relaxation of octahedrally coordinated mononuclear Fe(III)-, Co(II)-, and Mn(III)-containing polyoxometalates. Chem. Commun. (Camb.) *51*, 4081–4084.

67. Varga, F., Rajnák, C., Titiš, J., Moncoľ, J., and Boča, R. (2017). Slow magnetic relaxation in a Co(ii) octahedral-tetrahedral system formed of a $[CoL_3]^{2+}$ core with L = bis(diphenylphosphanoxido) methane and tetrahedral $[CoBr_4]^{2-}$ counter anions. Dalton Trans. *46*, 4148–4151.

68. Carlin, R.L., and Weissberger, E. (1964). Sulfur Donors: Cobalt(II) with Chelating Alkyl Sulfides. Inorg. Chem. *3*, 611–612.

69. Flint, C.D., and Goodgame, M. (1968). Studies of some metal complexes with chelating alkyl sulphides as ligands. J. Chem. Soc. A, 2178–2182.

70. Jiang, F., Siegler, M.A., Sun, X., Jiang, L., Fonseca Guerra, C., and Bouwman, E. (2018). Redox Interconversion between Cobalt(III) Thiolate and Cobalt(II) Disulfide Compounds. Inorg. Chem. *57*, 8796–8805.

71. Singh, M.K., Das, A., and Paul, B. (2009). Synthesis and characterization of mixed ligand complexes of cobalt(II) with some nitrogen and sulfur donors. J. Coord. Chem. *62*, 2745–2754.

72. O'Connor, J.E., and Amma, E.L. (1969). Crystal and molecular structure of trans-dichlorotetrakis(thiourea) cobalt(II). Inorg. Chem. *8*, 2367–2374.

73. Zabrodsky, H., Peleg, S., and Avnir, D. (1992). Continuous symmetry measures. J. Am. Chem. Soc. *114*, 7843–7851.

74. Karasawa, S., Yoshihara, D., Watanabe, N., Nakano, M., and Koga, N. (2008). Formation of monometallic single-molecule magnets

with an Stotal value of 3/2 in diluted frozen solution. Dalton Trans. (11), 1418–1420.

75. Sano, Y., Tanaka, M., Koga, N., Matsuda, K., Iwamura, H., Rabu, P., and Drillon, M. (1997). Formation of Ferromagnetic Chains by Photolysis of 1:1 Complexes of Bis(hexafluoroacetylacetonato)copper(II) with Diazodi-4-pyridylmethane. J. Am. Chem. Soc. *119*, 8246–8252.

76. Shinji, K., Satoru, K., Motohiro, N., and Noboru, K. (2006). Magnetic Properties of 1:4 Complexes of CoIIX2 (X = NCO−, NCS−, and Br−) with 4-(N-tert-Butylaminoxyl)pyridine. Antiferromagnets in Crystalline States and Single-Molecule Magnets in Frozen Solutions. Bull. Chem. Soc. Jpn. *79*, 1372–1382.

77. Díaz-Torres, R., Menelaou, M., Roubeau, O., Sorrenti, A., Brandariz-de-Pedro, G., Sañudo, E.C., Teat, S.J., Fraxedas, J., Ruiz, E., and Aliaga-Alcalde, N. (2016). Multiscale study of mononuclear Co^{II} SMMs based on curcuminoid ligands. Chem. Sci. (Camb.) *7*, 2793–2803.

78. Zhu, Y.-Y., Cui, C., Zhang, Y.-Q., Jia, J.-H., Guo, X., Gao, C., Qian, K., Jiang, S.-D., Wang, B.-W., Wang, Z.-M., et al. (2013). Zero-field slow magnetic relaxation from single Co(ii) ion: a transition metal single-molecule magnet with high anisotropy barrier. Chem. Sci. (Camb.) *4*, 1802–1806.

79. Bazhenova, T.A., Zorina, L.V., Simonov, S.V., Mironov, V.S., Maximova, O.V., Spillecke, L., Koo, C., Klingeler, R., Manakin, Y.V., Vasiliev, A.N., and Yagubskii, E.B. (2020). The first pentagonal-bipyramidal vanadium(III) complexes with a Schiff-base N_3O_2 pentadentate ligand: synthesis, structure and magnetic properties. Dalton Trans. *49*, 15287–15298.

80. Gupta, T., and Rajaraman, G. (2016). Modelling spin Hamiltonian parameters of molecular nanomagnets. Chem. Commun. (Camb.) *52*, 8972–9008.

81. Idešicová, M., Titiš, J., Krzystek, J., and Boča, R. (2013). Zero-field splitting in pseudotetrahedral Co(II) complexes: a magnetic, high-frequency and -field EPR, and computational study. Inorg. Chem. *52*, 9409–9417.

82. Mondal, A.K., Sundararajan, M., and Konar, S. (2018). A new series of tetrahedral Co(ii) complexes $[CoLX_2]$ (X = NCS, Cl, Br, I) manifesting single-ion magnet features. Dalton Trans. *47*, 3745–3754.

83. Sottini, S., Poneti, G., Ciattini, S., Levesanos, N., Ferentinos, E., Krzystek, J., Sorace, L., and Kyritsis, P. (2016). Magnetic Anisotropy of Tetrahedral Co^{II} Single-Ion Magnets: Solid-State Effects. Inorg. Chem. *55*, 9537–9548.

84. Krzystek, J., Zvyagin, S.A., Ozarowski, A., Fiedler, A.T., Brunold, T.C., and Telser, J. (2004). Definitive spectroscopic determination of zero-field splitting in high-spin cobalt(II). J. Am. Chem. Soc. *126*, 2148–2155.

85. Schmidt, S.F.M., Koo, C., Mereacre, V., Park, J., Heermann, D.W., Kataev, V., Anson, C.E., Prodius, D., Novitchi, G., Klingeler, R., and Powell, A.K. (2017). A Three-Pronged Attack To Investigate the Electronic Structure of a Family of Ferromagnetic Fe_4Ln_2 Cyclic Coordination Clusters: A Combined Magnetic Susceptibility, High-Field/High-Frequency Electron Paramagnetic Resonance, and ^{57}Fe Mössbauer Study. Inorg. Chem. *56*, 4796–4806.

86. Brown, P.J.M. (2009). CCSL User Manual. https://www.ill.eu/sites/ccsl/html/ccsldoc.html.

87. Ridier, K., Gillon, B., Gukasov, A., Chaboussant, G., Cousson, A., Luneau, D., Borta, A., Jacquot, J.-F., Checa, R., Chiba, Y., et al. (2016). Polarized Neutron Diffraction as a Tool for Mapping Molecular Magnetic Anisotropy: Local Susceptibility Tensors in Co(II) Complexes. Chemistry *22*, 724–735.

88. Neese, F. (2012). The ORCA program system. Wiley Interdiscip. Rev. Comput. Mol. Sci. *2*, 73–78.

89. Chilton, N.F., Anderson, R.P., Turner, L.D., Soncini, A., and Murray, K.S. (2013). PHI: a powerful new program for the analysis of anisotropic monomeric and exchange-coupled polynuclear d- and f-block complexes. J. Comput. Chem. *34*, 1164–1175.

90. Stoll, S., and Schweiger, A. (2006). EasySpin, a comprehensive software package for spectral simulation and analysis in EPR. J. Magn. Reson. *178*, 42–55.

91. Ferentinos, E., Xu, M., Grigoropoulos, A., Bratsos, I., Raptopoulou, C.P., Psycharis, V., Jiang, S.-D., and Kyritsis, P. (2019). Field-induced slow relaxation of magnetization in the S = 3/2 octahedral complexes trans-[Co{(OPPh2)(EPPh2)N}2(dmf)2], E = S, Se: effects of Co–Se vs. Co–S coordination. Inorg. Chem. Front. *6*, 1405–1414.

92. Drakopoulou, L., Raptopoulou, C.P., Terzis, A., and Papaefstathiou, G.S. (2010). Hydrogen-Bonded Networks Based on Cobalt(II), Nickel(II), and Zinc(II) Complexes of N,N′-Diethylurea. Bioinorg. Chem. Appl. *2010*, 12.

93. Kuz'mina, N.E., Palkina, K.K., Savinkina, E.V., Biryukov, D.A., and Kozlova, I.A. (2001). Complexation of cobalt iodide with urea under the conditions of ligand deficiency. Zhurnal Neorganicheskoj Khimii *46*, 1324–1331.

94. Herchel, R., Váhovská, L., Potočňák, I., and Trávníček, Z. (2014). Slow Magnetic Relaxation in Octahedral Cobalt(II) Field-Induced Single-Ion Magnet with Positive Axial and Large Rhombic Anisotropy. Inorg. Chem. *53*, 5896–5898.

95. Thiel, A.M., Damgaard-Møller, E., and Overgaard, J. (2020). High-Pressure Crystallography as a Guide in the Design of Single-Molecule Magnets. Inorg. Chem. *59*, 1682–1691.

96. Clark, R.C., and Reid, J.S. (1995). The analytical calculation of absorption in multifaceted crystals. Acta Crystallogr. *51*, 887–897.

97. Sheldrick, G.M. (2008). A short history of SHELX. Acta Crystallogr. A *64*, 112–122.

98. Skourski, Y., Kuz'min, M.D., Skokov, K.P., Andreev, A.V., and Wosnitza, J. (2011). High-field magnetization of Ho2Fe17. Phys. Rev. B *83*.

99. Bauer, B., Carr, L.D., Evertz, H.G., Feiguin, A., Freire, J., Fuchs, S., Gamper, L., Gukelberger, J., Gull, E., Guertler, S., et al. (2011). The ALPS project release 2.0: open source software for strongly correlated systems. J. Stat. Mech. *2011*, P05001.

100. Sandvik, A.W. (1999). Stochastic series expansion method with operator-loop update. Phys. Rev. B *59*, R14157–R14160.

101. Gukasov, A., and Brown, P.J. (2002). Determination of atomic site susceptibility tensors from polarized neutron diffraction data. J. Phys. Condens. Matter *14*, 8831–8839.

102. Gillon, B. (2007). La technique classique du rapport de flipping. Application aux aimants moléculaires et aux aimants photo-commutables. Collection de la Société Française de la Neutronique *7*, 13–40.

103. Klahn, E.A., Gao, C., Gillon, B., Gukasov, A., Fabrèges, X., Piltz, R.O., Jiang, S.-D., and Overgaard, J. (2018). Mapping the Magnetic Anisotropy at the Atomic Scale in Dysprosium Single-Molecule Magnets. Chemistry *24*, 16576–16581.

104. Borta, A., Gillon, B., Gukasov, A., Cousson, A., Luneau, D., Jeanneau, E., Ciumacov, I., Sakiyama, H., Tone, K., and Mikuriya, M. (2011). Local magnetic moments in a dinuclear Co2+ complex as seen by polarized neutron diffraction:Beyond the effective spin-1/2 model. Phys. Rev. B *83*, 184429.

105. Iasco, O., Chumakov, Y., Guégan, F., Gillon, B., Lenertz, M., Bataille, A., Jacquot, J.-F., and Luneau, D. (2017). Mapping the Magnetic Anisotropy inside a Ni4 Cubane Spin Cluster Using Polarized Neutron Diffraction. Magnetochemistry *3*, 25.

106. Ridier, K., Mondal, A., Boilleau, C., Cador, O., Gillon, B., Chaboussant, G., Le Guennic, B., Costuas, K., and Lescouëzec, R. (2016). Polarized Neutron Diffraction to Probe Local Magnetic Anisotropy of a Low-Spin Fe(III) Complex. Angew. Chem. Int. Ed. Engl. *55*, 3963–3967.

107. Chakoumakos, B.C., Cao, H., Ye, F., Stoica, A.D., Popovici, M., Sundaram, M., Zhou, W., Hicks, J.S., Lynn, G.W., and Riedel, R.A. (2011). Four-circle single-crystal neutron diffractometer at the High Flux Isotope Reactor. J. Appl. Cryst. *44*, 655–658.

108. Gukasov, A., Goujon, A., Meuriot, J.-L., Person, C., Exil, G., and Koskas, G. (2007). Super-6T2, a new position-sensitive detector polarized neutron diffractometer. Physica B *397*, 131–134.

109. Edwards, A.J. (2011). Neutron Diffraction – Recent Applications to Chemical Structure Determination. Aust. J. Chem. *64*, 869–872.

110. Dolomanov, O.V., Bourhis, L.J., Gildea, R.J., Howard, J.A.K., and Puschmann, H. (2009). OLEX2: a complete structure solution, refinement and analysis program. J. Appl. Cryst. *42*, 339–341.